Hindawi
Advances in Civil Engineering
Volume 2019, Article ID 5020357, 14 pages
https://doi.org/10.1155/2019/5020357

Research Article

The Activity of the Yaziba Fault on the Lower Reaches of the Jinsha River, Southwestern China: Indirect Evidence from Paleo Earthquakes and Ancient Landslides

Yulong Cui,[1,2] **Jianhui Deng**,[2] **and Chong Xu**[3]

[1]*School of Civil Engineering and Architecture, Anhui University of Science and Technology, Huainan 232001, Anhui, China*
[2]*State Key Laboratory of Hydraulics and Mountain River Engineering, Sichuan University, Chengdu 410071, China*
[3]*Key Laboratory of Active Tectonics and Volcano, Institute of Geology, China Earthquake Administration, Beijing 100029, China*

Correspondence should be addressed to Yulong Cui; ylcui@aust.edu.cn

Received 7 March 2019; Revised 20 April 2019; Accepted 5 May 2019; Published 19 May 2019

Academic Editor: Hayri Baytan Ozmen

In this paper, in order to confirm the strong activity of the Yaziba Fault and provide information needed for disaster prevention and mitigation and safety of the reservoir, we use field investigations and remote sensing interpretations to obtain the geometry of the Yaziba Fault and the distribution of the associated nearby landslides. Several new events are dated, and the paleo earthquake events in the fault area and their time intervals are analyzed along with previously dated events. Then, a typical landslide case is analyzed, and its instability is determined using the limit equilibrium method. The main results of our study are as follows: (1) the Yaziba Fault extends for 20 km; (2) 164 landslides have occurred in the fault area, the LND reached 0.1 km^{-2}, and the LAP reached 0.07 for the entire research area, and the LND and LAP gradually decrease with increasing distance from the Yaziba Fault; (3) 39 dating dates are obtained and 19 paleo earthquakes are concluded, from which the time interval of earthquakes shortened from 147,000 to 3800 years ago is found; and (4) the Daomakan landslide had a 0.6 g horizontal seismic acceleration, which indicates that it was an earthquake landslide. This comprehensive method combined the geometric characteristics of the fault, paleo earthquake data, the regional landslide distribution, and the geotechnical engineering analysis of typical landslides in the area to indirectly determine the fault's activity and provide a reference for the study of fault activity in mountainous areas.

1. Introduction

Earthquakes in mountainous areas and the landslides they trigger pose a significant risk to human life and property [1–4]. For example, (i) in 1786, an *M* 7.75 earthquake occurred in the Kangding-Luding area in southwestern China, causing a landslide that blocked the Dadu River and formed a barrier lake [5]; (ii) in 1933, an *M* 7.5 earthquake in Diexi Town, southwestern China, triggered a large number of landslides and formed more than 10 landslide dams and dammed lakes [6]; and (iii) in 2008, the Wenchuan *M* 7.9 earthquake produced a large number of landslides and barrier lakes [7]. Therefore, the medium-long-term prediction of earthquakes is of great significance to disaster prevention and reduction in mountainous areas.

Fault activity evaluation is the most important basis for the medium-long-term prediction of earthquakes. Most research methods use the deep geophysical field [8] and the geometric characteristics of fault, including the length of the surface rupture, the fault offset [9], the timing of fault activity [10], and surface deformation [11], to qualitatively evaluate the fault. Some scholars have tried to identify quantitative indicators and make quantitative evaluations using probability theory [12, 13]. Two important indicators of fault activity are intensity, which is estimated from the magnitude of the earthquake, and frequency, which is determined from the timing of fault activity. The activity intensity is usually calculated based on historical seismic records [14, 15], but it can also be analyzed from seismic traces, e.g., landslides [16, 17], buildings destroyed by

earthquakes, [18], and standing orphans [19]. These seismic traces are used to calculate the seismic peak acceleration, which is used to determine the possible seismic fault events and their magnitudes as well as tectonic environment of the site [18, 20–22]. The timing of fault activity is mainly obtained through various dating methods, such as the direct testing of fault gouges in the fault zone [10, 23] or the indirect testing of earthquake artifacts. Frequently used earthquake artifacts include ancient landslides [24, 25] and sediments from barrier lakes [26, 27]. These earthquake artifacts, which can provide information about fault activity, seismic landslides, and barrier lakes, are undoubtedly the most common and reliable ones because large earthquakes in mountain areas often produce a large number of large landslides, which can block rivers and form barrier lakes. These artifacts provide abundant information we can use to understand the related fault activity. Nevertheless, the study of fault activity using seismic landslides is still not well developed, and more case studies are needed to promote the further development of this method.

The Yaziba Fault is located on the Jinsha River between Sichuan and Yunnan only 19 km downstream of the Xiluodu hydropower station. This hydropower station is the largest station on the Jinsha River, has the second largest power generation capacity in China, and is ranked as the third largest in the world. Its dam is 285.5 m high, which makes it the third highest arch dam in China. The Yaziba Fault intersects the Jinsha River several times, so there are several well-developed ancient landslides near the river. Due to the construction of large hydropower stations on the river, there have been many studies on the geology, earthquakes, and landslides in this area, but several questions regarding the seismic hazards associated with this fault remain unsolved. In this paper, geological surveys and tracing and remote sensing interpretations of ancient landslides are used to determine the geometry of the fault and the nearby associated landslides. A variety of geological dating methods, along with previous dates, are employed to infer the distribution of paleo earthquakes around the fault. The results provide valuable information that can increase our understanding of the seismicity, earthquake prediction, and safe operation of hydropower stations in the region. The research methods used can also provide a reference for fault activity research in other similar mountainous areas.

2. Study Area

The lower part of the Jinsha River (Panzhihua-Yibin) in China is 782 km long, with a natural drop in the elevation of 729 m, which provides abundant hydropower resources. Along this section of the river, four hydropower stations have been constructed in a cascading manner: the 8.7 million·kW Wudongde power station, the 12 million·kW Baihetan power station, the 12.6 million·kW Xiluodu power station, and the 6 million·kW Xiangjiaba power station (Figure 1).

The Yaziba Fault is located between the Xiluodu and Xiangjiaba power stations. Tectonically, the fault is located on the slope of the transition from western Sichuan and the northern Yunnan Plateau on the eastern margin of the Tibetan Plateau to the Sichuan Basin in the east. This region ranges in elevation from 300 to 3000 m, making it an intermediate-high mountainous area with a large topographic relief. The Jinsha River flows from south to north. The strong incision of the river has produced steep terrain with many deep narrow valleys with cliffs in many areas. Most of the Jinsha River valleys are narrow V-shaped or U-shaped valleys with bank slope gradients of 30°–60° and maximum slope heights of up to 600 m. The Carboniferous, Devonian, Cretaceous, and Tertiary strata are absent, but all of the other strata from the Upper Proterozoic to the Cenozoic are exposed in the area. The lithology of the area is dominated by limestone, sandstone, dolomite, basalt, and shale.

The Yingjing-Mabian-Yanjin fault zone, which contains the Yaziba Fault, is a complex seismic zone on the eastern side of the boundary between Sichuan and Yunnan, which strikes NNW and extends downward to the Moho interface. Based on its surface expression, it is composed of nine major secondary faults (Figure 2), i.e., the Tianquan-Xingjing, Ebian, Lidian, Zhongdu, Manao, Yaziba, Guancun, Zhongcun, and Dianlanba Faults. In the southern section, the Dianlanba, Manao, Yaziba, Zhongdu, Guancun, and Zhongcun Faults collectively make up the Mabian-Daguan fault zone (Figure 2). Many studies have been conducted on this fault zone. The Yaziba Fault is an important component of this feature (Figure 2), which extends approximately parallel to the Jinsha River and crosses the river twice. Previous dating shows that it has been active since the Quaternary, and a large number of ancient landslides and barrier lakes have been identified on both sides of the fault.

Since 1900, 30 M 5.0 or greater earthquakes have occurred on the Yingjing-Mabian-Yanjin fault zone, including 6 M 6.0–6.9 events and one M 7.1 event, i.e., the 1974 Daguan-Yongshan shock. Major earthquakes have also occurred near the Yaziba Fault, e.g., the 1216 M 7.0 Mahu and 1844 M 7.0 Daguanbei earthquakes (Figure 2).

3. Methods and Data

3.1. Investigation of the Yaziba Fault and Landslides. In this study, we had determined the geometry of the fault and landslides based on field investigations and remote sensing interpretations. We used observations and mapping to investigate the Yaziba Fault along strike and for several cross sections at key sites. For the landslides, their planar ranges were delineated using remote sensing interpretations, which were then corrected based on on-site observations and measurements. In addition, the lithology and structure of the landslides were determined. The landslides were interpreted using the Google Earth platform and images. The defined landslide surfaces were converted to kmz files using the Google Earth platform, and then, they were translated into shape files using the ArcGIS platform. The plotting and analysis were also conducted using the ArcGIS platform. The other basic maps used in this study include a 1 : 50,000 topographic map, its digital terrain DEM, and a 1 : 200,000 Leibo geologic map.

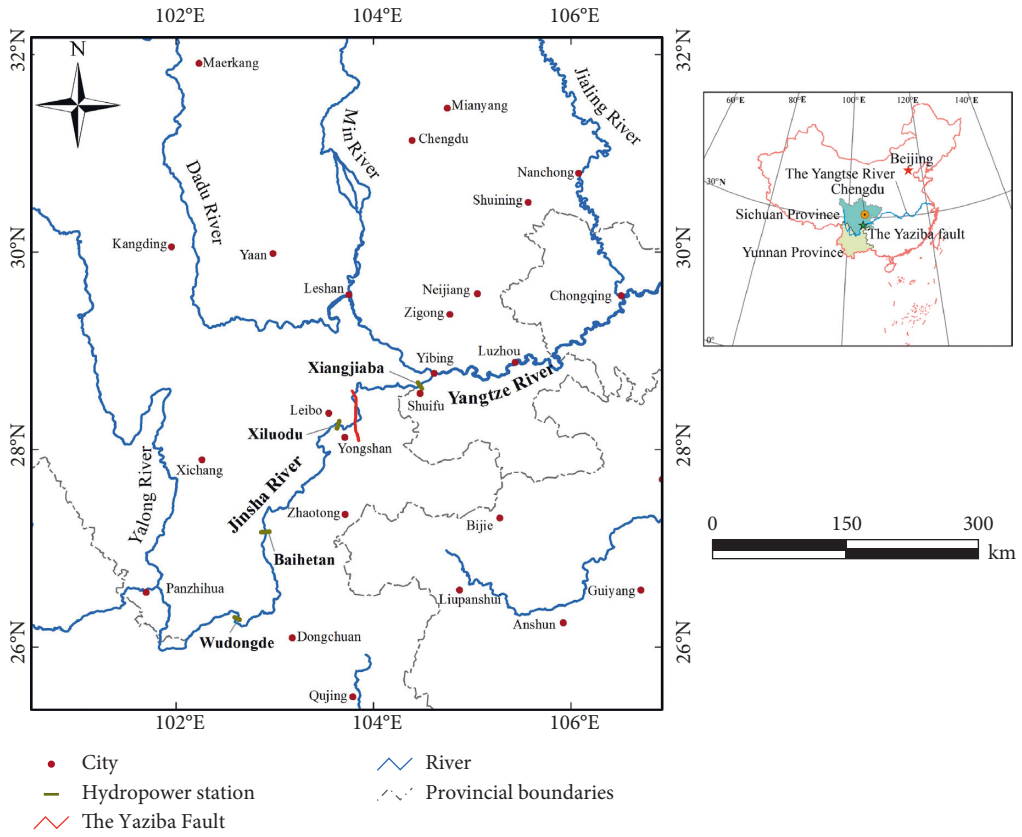

Figure 1: Map showing the location of the study area.

3.2. Acquisition of Geochronologic Data. The geochronologic data were obtained from both historical records of earthquakes and geologic dating. The geologic dating included two methods: the direct method involves the direct analysis of materials inside the fault zone, including fault gouges and fault breccia, while the indirect method involves the analysis of earthquake artifacts, e.g., the liquefaction of sandy soil and the presence of landslides and barrier lakes. The dating techniques used in this study include thermoluminescence (TL), scanning electron microscopy (SEM), electron spin resonance (ESR), radiocarbon dating (^{14}C), optically stimulated luminescence (OSL), and ^{36}Cl cosmogenic nuclide exposure methods. Sixteen of the geochronologic dates are from previous studies, and 23 new dates were obtained. Of these 23 new dates, 10 were obtained using the ^{36}Cl method, 10 were obtained using the ESR method, and 3 were obtained using the OSL method. Several field photos are shown in Figure 3.

The ^{36}Cl samples were tested at the accelerator mass spectrometry (AMS) facility in the Ion Beam Physics Laboratory of Swiss Federal Institute of Technology Zurich (ETH Zurich). The pretreatment and preparation were performed using the isotope dilution method [28]. The sample processing and analysis were conducted using the methods of Ivy-Ochs et al. [24, 29]; and the dating calculations were the same as those described by Ivy-Ochs et al. [24, 29] and Claude et al. [30].

The ESR samples were analyzed at the Division of Radiation Metrology, China Institute of Atomic Energy, using an EMX model spectrometer made by the German BRUKER company. The normal quantifier was an alanine thin film dosimeter with a dose rate of 20 Gy·min^{-1}.

The OSL samples were analyzed at the Groundwater, Mineral water, and Environment Monitoring Center of China. The treated samples were analyzed using a Daybreak 2200 OSL instrument made in the United States. The dose rate of the 90Sr-Y beta radiation source was approximately 0.086273 Gy/sec. All of the samples were regenerated using simple multislice regeneration of the fine particles to obtain equivalent dose values and were fitted using the saturation index method.

4. Results and Analysis

4.1. Geometry of the Yaziba Fault. The available data indicate that the Yaziba Fault strikes approximately NS, dips 70°–80° west, and extend for 30 km (Figure 4). It is a regional reverse fault with a 200–400 m displacement that primarily cuts the Triassic strata, but at its southern end, it extends down into the Sinian strata. From south to north, this fault stretches along the Changping River (a tributary of the Jinsha River) that crosses the Jinsha River and extends along a ridge to the mountaintop on the left bank, turning at the top. Then, it extends along a gully, arriving back at the Jinsha River, runs along the left bank for 10 km, and crosses the Jinsha River for the second time before entering the mountain on the right bank (Figure 4). According to our site survey, the fault does follow this path. However, we found that as claimed by previous studies, at its northern end, the fault continues to

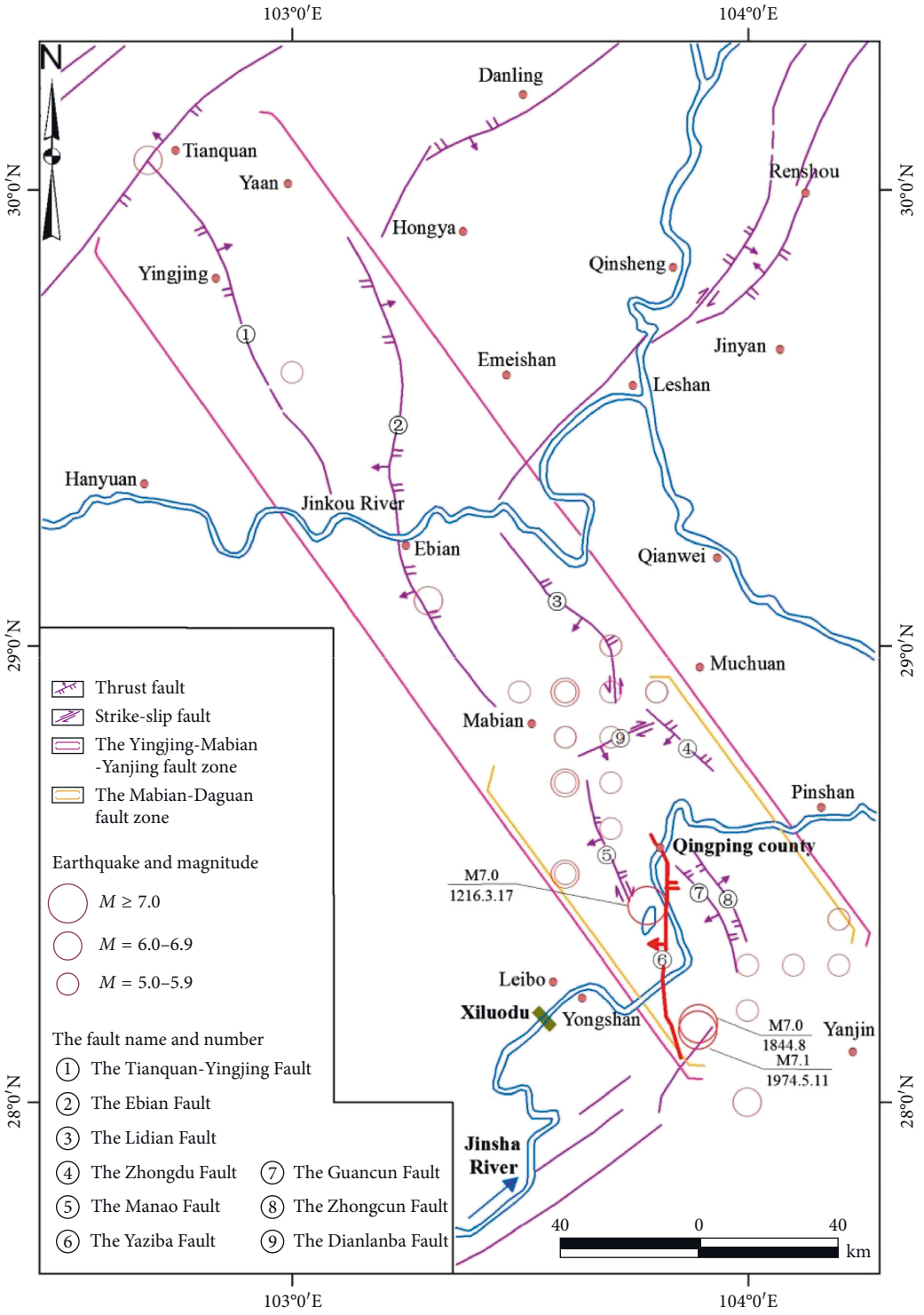

Figure 2: Map showing the locations of the Yingjing-Mabian-Yanjing fault zone and the Yaziba Fault.

extend northward for approximately 20 km (Figure 4). The main evidence for this is the discovery of breccia, fault gouge, and springs in this area (Figure 5). Figure 5(d) shows the river valley landforms of the region where the fault crosses the Jinsha River. To illustrate its structure, a cross section was constructed (Figure 6). This cross section shows that the fault cuts the lower Permian strata and the Permian Emeishan basalt. It is a thrust fault that dips 70° to the west. In addition, the landform to the northwest of the observed fault is a gully, implying that the fault may extend even farther. We speculate that the fault may connect to other faults in the Yingjing-Mabian-Yanjin Fault zone, such as No. 5 Manao Fault (Figure 2). Thus, the total fault length will be more than 50 km. Based on the China Geological Survey's [31] classification criteria for fault activity, if the length of an active fault is used as the classification index, when the

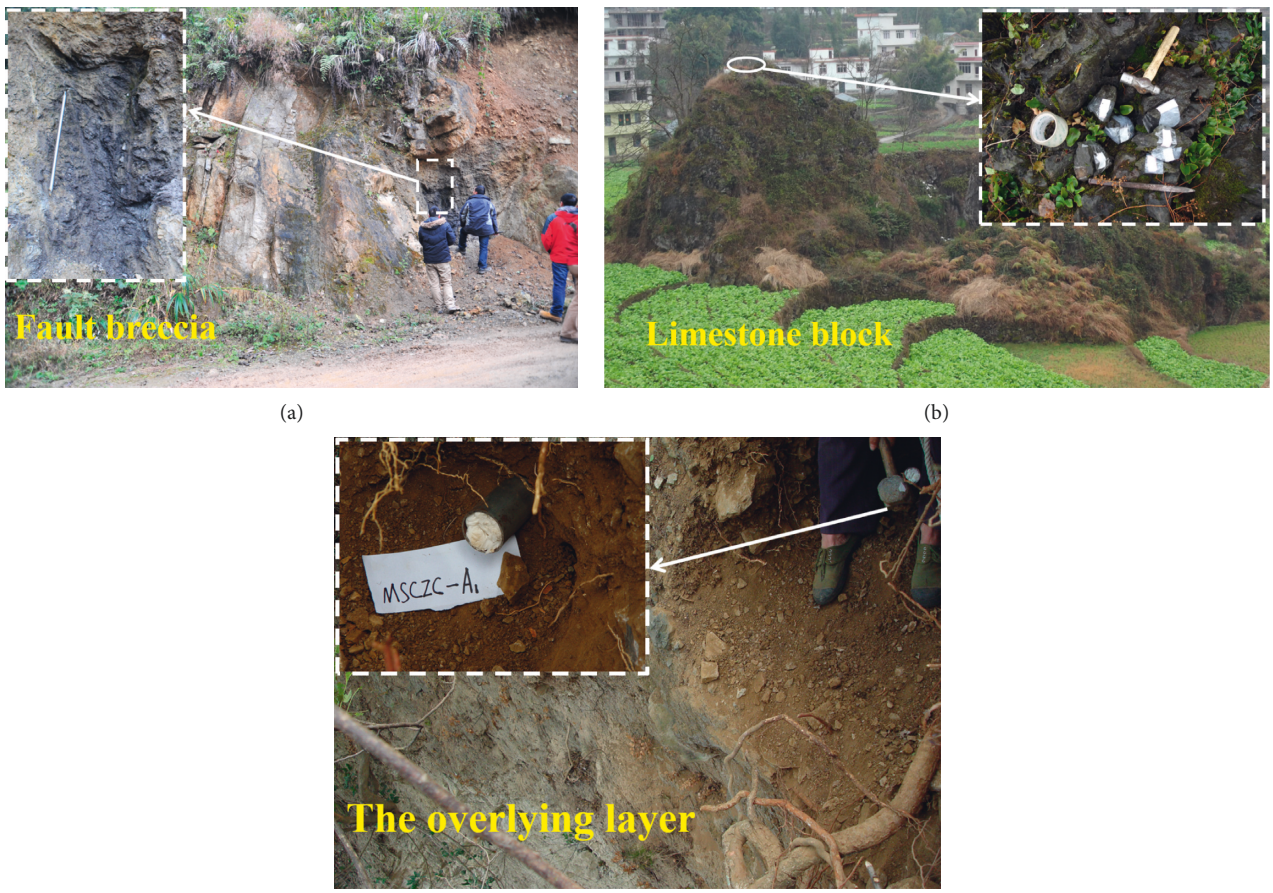

Figure 3: On-site photos of samples. (a) The ESR test, (b) the ^{36}Cl exposure test, and (c) the OSL test.

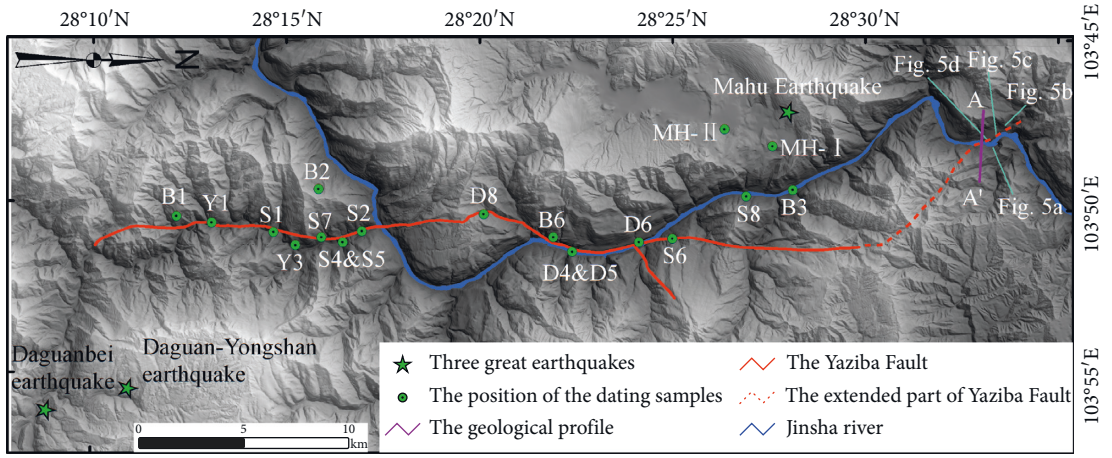

Figure 4: Map showing the Yaziba Fault, the sampling sites for dating, and the epicenter of three great earthquakes with $M > 7.0$.

length of the fault is adjusted from 30 km to 50 km, the activity of the Yaziba Fault increases by one level, from weak activity to medium activity.

4.2. Paleo Earthquakes around the Fault. As was previously stated, 39 dates were used in this study (Table 1). Of these dates, 8 samples were for fault gouges and fault breccia, 18 were for landslides, 10 were for liquefied sandy soils and Quaternary overburden beds, and 3 were for barrier lakes. Eight samples were dated using TL, 2 samples were dated using SEM, 13 samples were dated using ESR, 2 samples were dated using ^{14}C, 4 samples were dated using OSL, and 10 samples were dated using ^{36}Cl. To properly consider the errors in each dating method and their large differences in accuracy, the data were analyzed, screened, and merged

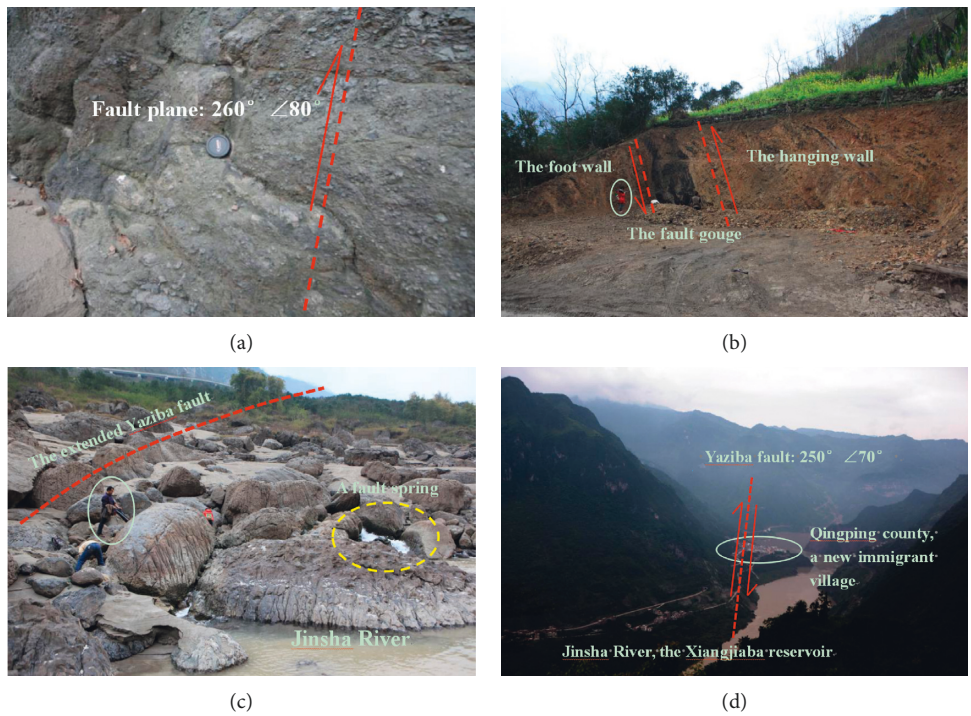

FIGURE 5: Some evidence for the newly discovered part of the Yaziba Fault. (a) The fault breccia on the right bank of the Jinsha River, (b) the fault gouge on the left bank of the Jinsha River, (c) a spring on the fault zone, and (d) the Jinsha River valley that the Yaziba Fault passes through. See Figure 4 for locations.

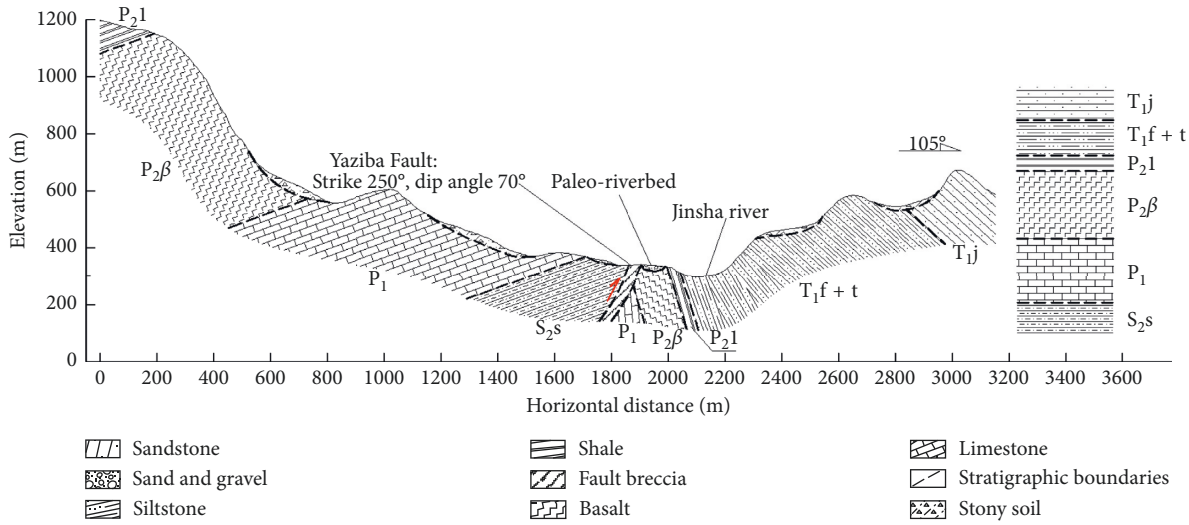

FIGURE 6: Cross section A-A′. See Figure 4 for its location. S_2s: Silurian Shimenkan formation, P_1: lower Permian strata, $P_2\beta$: Permian Emeishan basalt, P_2l: Permian Leping formation, T_1f+t: Triassic Feixianguan and Tongjiezi formations, and T_1j: Triassic Jialingjiang formation.

before it was used to identify paleo earthquakes. As shown in Table 1, samples D1 (80.9 ka) and D5 (81 ka) are adjacent, which indicates that these samples may be from the same earthquake; while sample D3 is Q_3, (126–11.7 ka), and thus an earthquake occurred before 81 ka. Samples B1 (113 ka) and B6 (115 ka) represent two landslides that may have been formed by the same earthquake, so a seismic event occurred before 113 ka. Samples S4 and S5 are both from lacustrine sediments near the fault, and the TL and OSL dating results are adjacent, so an earthquake occurred before 43.3–44.0 ka. Sample B16 (29.6 ka) is the average value of three samples with ages of 27.9 ka, 33.1 ka, and 27.7 ka. Sample MH-I (20.8 ka) represents the first event, and sample MH-II (13.2 ka) represents the second event, which formed the Mahu landslide. These two ages were obtained from 10 samples using the ^{36}Cl cosmic nuclide exposure dating

Table 1: Age dates for the area around the Yaziba Fault.

Test object	Indicated age	Sample material	Number	Dating method	Age (ka)	Source
Fault gouge or fault breccia	The age of activity on the Yaziba Fault	Fault gouge	D1	TL	80.9 ± 15.3	Lin [32]
			D2	SEM	Q_2	Lin [32]
			D3	SEM	Q_3	Lin [32]
		Fault breccia	D4	ESR	147	Our test
		Fault breccia	D5	ESR	81	Our test
		Fault breccia	D6	ESR	14.2	Our test
		Calcite vein	D7	ESR	321 ± 32	Our test
		Fault gouge	D8	ESR	6.79 ± 0.03	Our test
Landslide	The age of the tested landslide	Breccia from the sliding belt	B1	ESR	113	Lin [32]
		Calcite vein	B2	TL	115 ± 14	Lin [32]
			B3	ESR	5	Lin [32]
		Limestone breccia	B4	ESR	1104 ± 124	Our test
		Limestone breccia	B5	ESR	1840 ± 190	Our test
		Limestone breccia	B6	ESR	29.59	Our test
		Limestone rock	MH-I	^{36}Cl	20.8	Our test
		Limestone rock	MH-II	^{36}Cl	13.2	Our test
The seismic liquefaction and the Quaternary overburden layer	The fault activity age	Carbon chips	S1	^{14}C	24.5 ± 0.8	Hou et al. [33]
	The age of the flood alluvial terrace	Wood charcoal	S2	^{14}C	28	Wang [34]
	The age of seismic liquefaction	Sandy soil	S3	ESR	260	Wang [34]
	The age of the river sediments	Silt	S4	TL	43.3 ± 3.3	Wang [34]
			S5	OSL	47 ± 0.5	Wang [34]
	The age of the ancient earthquake wedge	Clay	S6	TL	19.32 ± 1.64	[33]
	The age of the seismic liquefaction	Sandy soil	S7	TL	11.63 ± 0.99	Hou et al. [33]
	The age of the layer overlying the Yaziba Fault	Silt	S8	OSL	3.8 ± 0.03	Our test
Quake lake	The age of the tested Quake lake	Sandy soil	Y1	TL	15.69 ± 1.33	Hou et al. [33]
		Sandy soil	Y2	TL	7.06 ± 0.142	
		Sandy soil	Y3	TL	5.75 ± 0.49	

Test object	Indicated age	Sample material	Number	Dating method	Age ($\times 10^4$ year)	Source
Fault gouge or fault breccia	The activity age of the Yaziba Fault	Fault gouge	D1	TL	8.09 ± 1.53	Lin [32]
			D2	SEM	Q_2	Lin [32]
			D3	SEM	Q_3	Lin [32]
		Fault breccia	D4	ESR	14.7	Our test
		Fault breccia	D5	ESR	8.1	Our test
		Fault breccia	D6	ESR	1.42	Our test
		Calcite vein	D7	ESR	32.1 ± 3.2	Our test
		Fault gouge	D8	ESR	0.679 ± 0.003	Our test
Landslide	The age of the tested landslide	Breccia from the sliding belt	B1	ESR	11.3	Lin [32]
		Calcite vein	B2	TL	11.5 ± 1.4	Lin [32]
			B3	ESR	5.6	Lin [32]
		Limestone breccia	B4	ESR	110.4 ± 12.4	Our test
		Limestone breccia	B5	ESR	184 ± 19	Our test
		Limestone breccia	B6	ESR	2.959	Our test
		Limestone rock	MH-I	^{36}Cl	2.08	Our test
		Limestone rock	MH-II	^{36}Cl	1.32	Our test

Table 1: Continued.

Test object	Indicated age	Sample material	Number	Dating method	Age (ka)	Source
The seismic liquefaction and the Quaternary overburden layer	The fault activity age	Carbon chips	S1	^{14}C	2.45 ± 0.08	Hou et al. [33]
	The age of the flood alluvial terrace	Wood charcoal	S2	^{14}C	2.8	Wang [34]
	The age of the seismic liquefaction	Sandy soil	S3	ESR	26	Wang [34]
	The age of the river sediments	Silt	S4	TL	4.33 ± 0.33	Wang [34]
			S5	OSL	4.47 ± 0.05	Wang [34]
	The age of the ancient earthquake wedge	Clay	S6	TL	1.932 ± 0.164	Hou et al. [33]
	The age of the seismic liquefaction	Sandy soil	S7	TL	1.163 ± 0.099	Hou et al. [33]
	The age of the overlying layer above the Yaziba Fault	Silt	S8	OSL	0.38 ± 0.03	Our test
Quake lake	The age of the tested Quake lake	Sandy soil	Y1	TL	1.569 ± 0.133	Hou et al. [33]
		Sandy soil	Y2	TL	0.706 ± 0.0142	
		Sandy soil	Y3	TL	0.575 ± 0.049	

B6 is an average value of three samples; S8 is an average value of three samples; MH-I is an average value of five samples; MH-II is an average value of five samples.

method, combined with geomorphological and lithological analysis of the Mahu landslide, so they are deemed reliable. Through these comparative analyses, relatively reliable ages were established for the paleo earthquakes that occurred around the fault since 147,000 years (Table 2). The locations of the dated samples presented in Table 2 are shown in Figure 4. The time intervals listed in Table 2 are plotted in Figure 7. As can be seen from the power function trend line in Figure 7, from 147,000 years to 3800 years ago, the time interval between earthquakes is becoming shorter.

In addition, historical records show that four major earthquakes occurred from 1216 to 1917 AD, i.e., the 1216 Mahu, 1844 Dabei, 1917 Jilipu, and 1974 Daguan earthquakes, which results in an average recurrence interval of 175 years. It should be noted that since 1844, the recurrence interval is only 43 years, indicating an enhancement trend of seismicity in this area.

4.3. Landslides on Both Sides of the Yaziba Fault. The research area is centered on the Yaziba Fault, extends for approximately 17 km to each side of the fault, and covers an area of 1660 km^2. In the study area, 164 landslides were identified from field surveys and remote sensing interpretations (Figure 8). Among them, four of the landslides (groups), i.e., the Mahu, Guancun, Damaotan, and Laizigou slope failures, have volumes on the scale of billions of m^3. The basic characteristics of the Mahu landslide have been described in [35]. Apparently, many landslides have occurred around the Yaziba Fault. Here, two commonly used statistical indices of landslide distribution, i.e., the landslide area percentage (LAP) and the landslide number density (LND) [1, 36], are used to analyze the relationship between these landslides and the Yaziba Fault:

$$\text{LAP} = \frac{A_l}{A_b}, \qquad \text{LND} = \frac{n_l}{A_b}, \tag{1}$$

where A_l is the landslides area in each zone, n_l is the number of landslides in each zone, and A_b is the area of each zone.

For the selected 33 km × 50 km rectangular study area, the LAP is 0.07 and the LND is 0.1 km^{-2}, which is higher than those for most mountainous areas. Taking the Yaziba Fault as the center line, the left and right sides can each be divided into five zones: 0–3 km, 3–6 km, 6–9 km, 9–12 km, and >12 km (Figure 8). Due to the large scale and complexity of the Mahu landslide [35], it was eliminated from the statistical analysis. The LAP and LND of each zone were calculated, and the results are shown in Figure 9. Figure 9(a) shows that on the left side of the fault, the LAP and LND gradually decrease from 0 to 6 km, increase from 6 to 9 km, and reach a peak value at >12 km, which is mainly caused by the Laizigou landslide group (Figure 8). Figure 9(b) shows that on the right side of the fault, the LAP and LND gradually decrease from 0 to 6 km, increase from 6 to 9 km, reach a peak value at 9–12 km, and decrease from >12 km. The peak value at 9–12 km is primarily caused by the landslides in area A in Figure 8. There could be a seismic fault in area A that caused the abundance of landslides. Generally speaking, the landslides are more developed in the 0–6 km zone on both sides of the Yaziba Fault. Based on relevant research on earthquake-triggered landslides [1, 37, 38], these landslides were most likely induced by paleo earthquakes caused by the Yaziba Fault.

Table 2: The 19 paleo earthquakes identified after analysis and screening.

Number	Dating method	Age (ka)	Time interval (ka)
D4	ESR	147	
B2	TL	115	3.2
B1	ESR	113	0.2
D5	ESR	81	3.2
B3	ESR	56	2.5
S5	OSL	44.7	1.13
S4	TL	43.3	0.14
B6	ESR	29.59	1.371
S2	^{14}C	28	0.159
S1	^{14}C	24.58	0.342
MH-I	^{36}Cl	20.8	0.378
S6	TL	19.32	0.148
Y1	TL	15.69	0.363
D6	ESR	14.2	0.149
MH-II	^{36}Cl	13.2	0.1
S7	TL	11.63	0.157
D8	ESR	6.79	0.484
Y3	TL	5.75	0.104
S8	OSL	3.8	0.195

MH-I is the first event of the Mahu landslide; MH-II is the second event of the Mahu landslide.

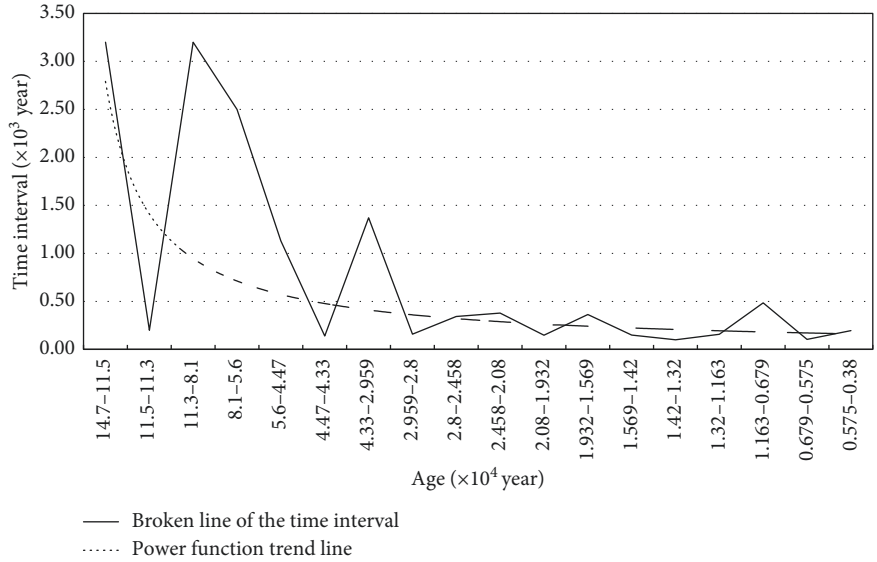

Figure 7: Broken line of the time interval and its power function trend line. The dates are from Table 2.

One of the landslides previously mentioned, the Daomakan landslide (Figure 10), exhibits characteristics typical of earthquake-induced slope failure, and it is only 2.9 km from the Yaziba Fault. The topography around this landslide is similar to a round-backed armchair, with a current slope of 59° toward the Jinsha River. The upper part of the slope is the back wall of the landslide, the sliding surface is the plane of the limestone bedrock, and the middle of the slope (380 m·a.s.l.) is the landslide deposit accumulation platform. Since the leading edge of the landslide has been eroded by the Jinsha River, the slope in the front is relatively gentle, approximately 15°–20°. The top of the head scarp is 500 m·a.s.l., and the leading edge of the residual deposit is 335 m·a.s.l., 5 m above the water surface of the Jinsha River. The volume of the residual landslide deposit is approximately $150 \times 10^4\ m^3$.

The landslide deposit consists of boulders and granular limestone soils with a low clay content, a relatively high gravel content, and rare large boulders. The bedrock of the slide bed is exposed at the front of the landslide (Figure 11), which is a fractured structure. Although the bedding structure of the original limestone is preserved, the bedding is disordered, indicating that the area was strongly compressed by tectonic movement before the landslide. The limit equilibrium method was used to determine how much seismic force was needed to cause slope instability. The equation of Dai et al. [16] was used:

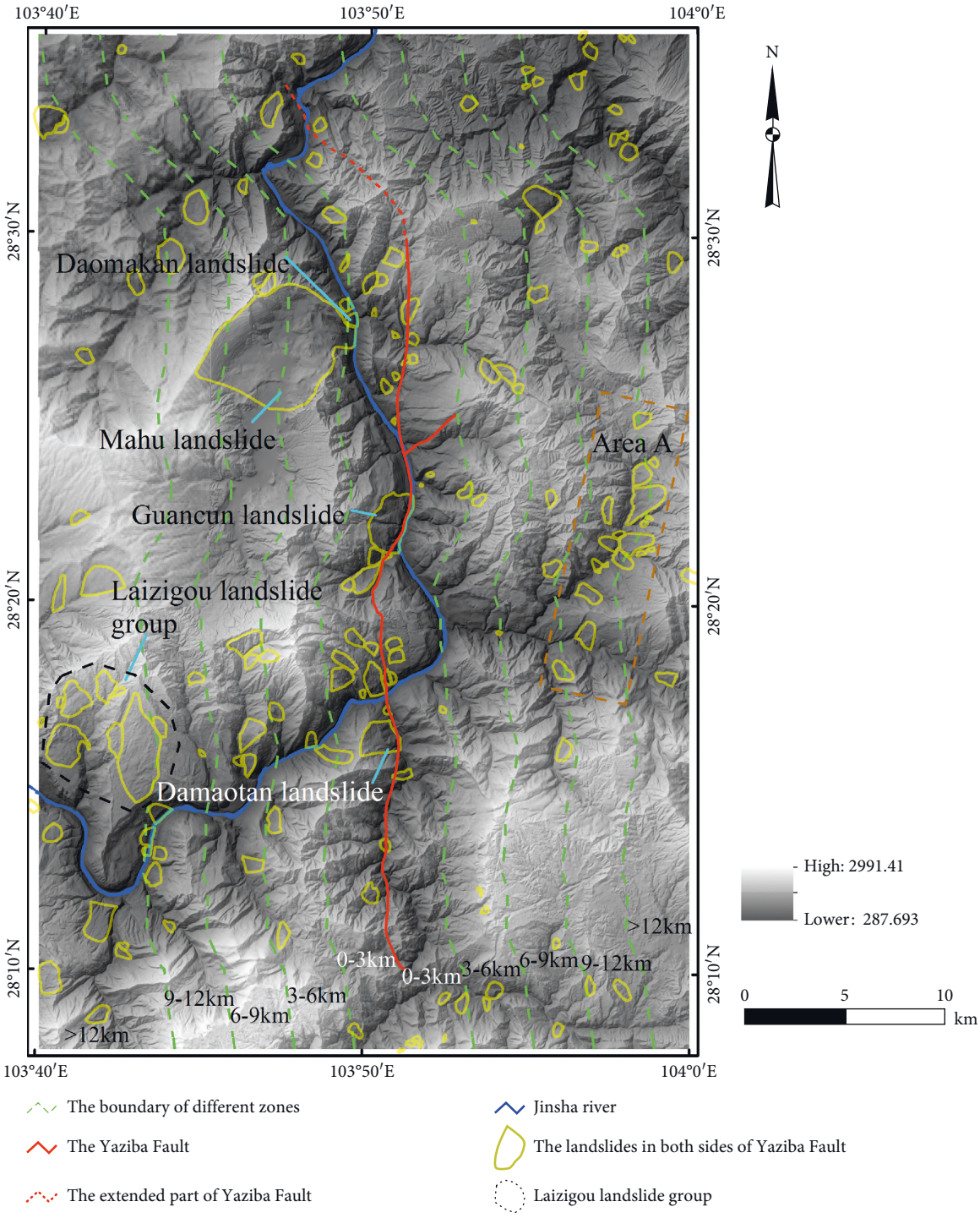

Figure 8: Landslides near the Yaziba fault.

$$a \approx \frac{\sum((cl_i + (w_i - u_i l_i)\tan\varphi)/(1 + \tan\alpha_i \tan\varphi)) - \sum w_i \sin\alpha_i}{\sum m_i \sin\alpha_i}, \quad (2)$$

where i is the slice index, a is the seismic acceleration (g), and g is the gravitational acceleration. Only the horizontal seismic acceleration was considered, while the vertical seismic acceleration was assumed as zero. c is the cohesion on the slide surface; φ is the internal friction angle on the slide surface; l is the bottom length; u is the pore water pressure on the bottom surface; and w is the gravity, m is the mass; and α is the angle between the tangent to the center of the base of each slice and the horizontal.

The computational model is shown in Figure 12, in which R is the radius of the circle considered in the slope stability analysis. Referring to the empirical values given by Shi-biao and Zhang [39], c is 0, the equivalent of φ is 60°, and u is ignored. The calculation indicates that a horizontal seismic

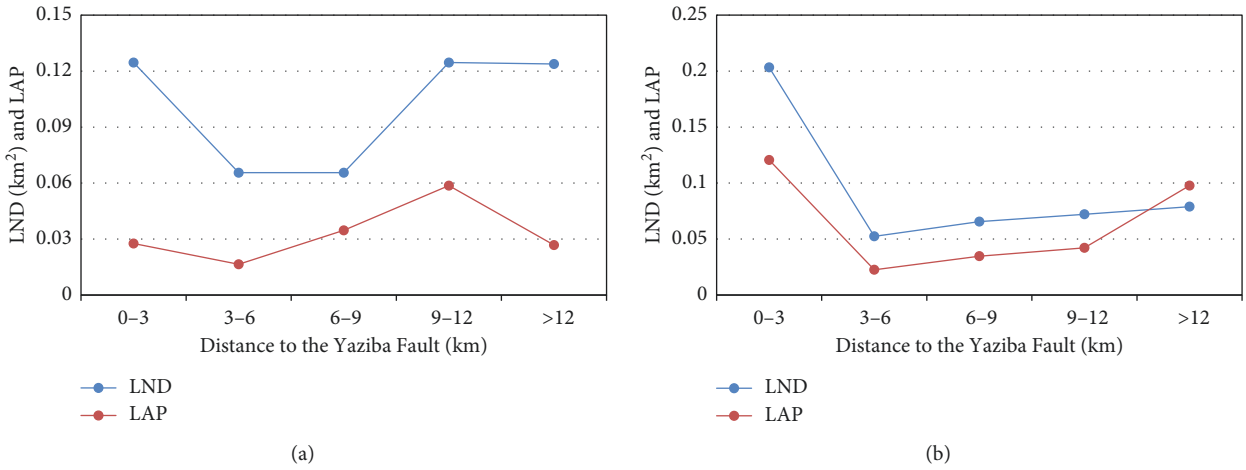

Figure 9: LND and LAP of different zones, i.e., different distances from the Yaziba Fault. (a) Left side of the fault, and (b) right side of the fault.

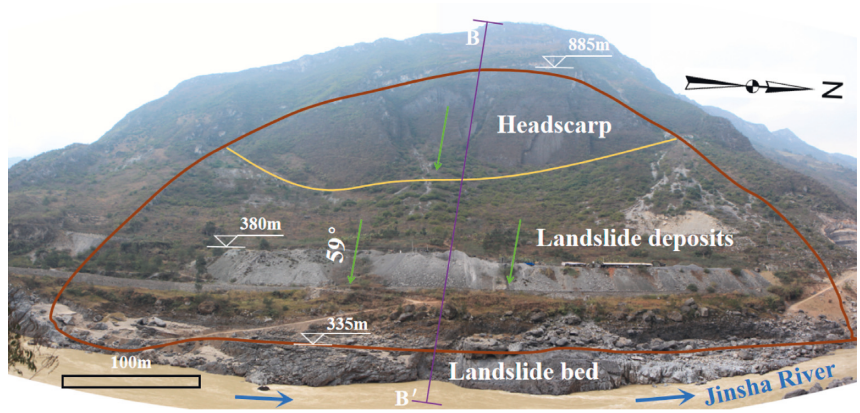

Figure 10: Panoramic view of the Daomakan landslide.

Figure 11: Daomakan landslide bed.

acceleration of 0.6 g is needed to cause landslide instability. In the absence of seismic force, if the bank slope slides, its equivalent φ should be as low as 38.5°, which is impossible for the limestone rock mass. Therefore, the Daomakan landslide was most likely induced by an earthquake.

5. Discussion

Previous studies of this region have yielded the following results. Liu [40] suggested that possible moderate-large earthquakes in the Mabian region would most likely cause earthquake swarms in the future. Li and Cheng [41] assumed that this fault zone was entering its fourth active period, and M 6 or greater earthquakes may occur in the next few years. Wang and Li [42] pointed out that there may be hidden deep faults beneath the fault zone. Hou et al. [33] analyzed the tectonic stress field of the Mabian-Daguan fault zone and revealed its complicated geologic structure. They concluded that the Yaziba Fault is a Holocene active fault, while most of the other faults were active during the Late and Middle Pleistocene. Ruan et al. [43] concluded that the potential for strong earthquakes exists in the southern part of the Yaziba Fault. Cheng [44] estimated that an M 6.75 earthquake may occur in the southern section of the Mabian-Daguan Fault zone.

Based on our field investigations, the length of the Yaziba Fault is extended from its previously determined 30 km to 50 km. Our analysis of 39 dated events around the fault suggests that 19 paleo earthquakes have occurred since 147,000 years ago. Finally, 164 landslides on both sides of the fault were identified from field investigations and interpretations of remote sensing data. The LAP accounts for 7.0% of the study area, which indicates that landslide

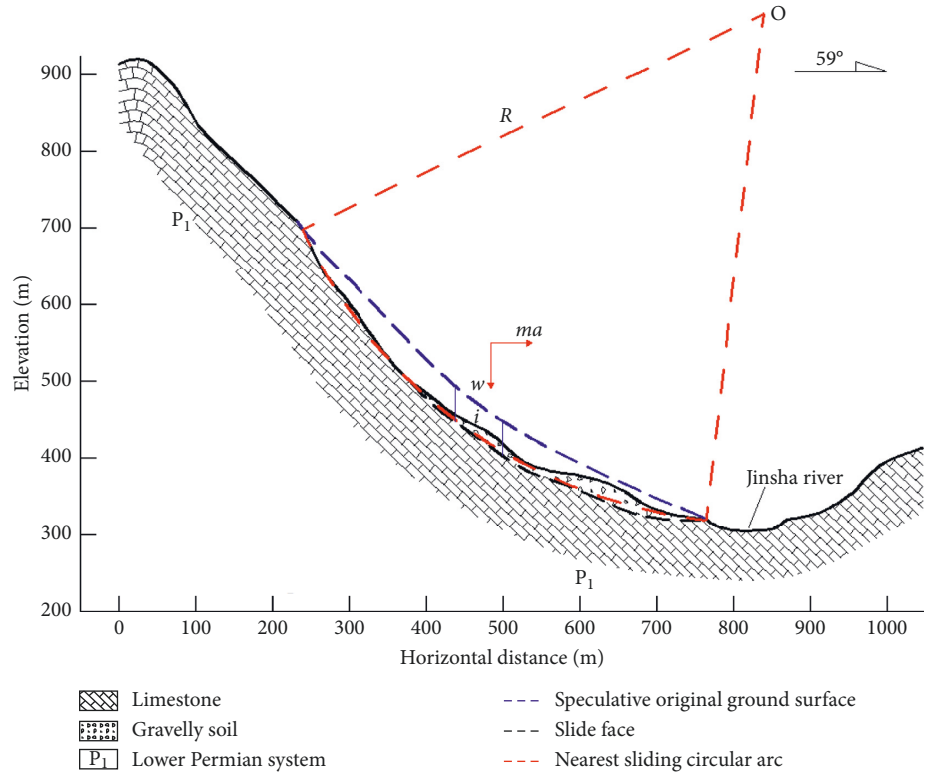

Figure 12: Cross section B-B′ at the center of the Daomakan landslide. The model from the limit equilibrium calculation. See Figure 10 for locations.

susceptibility is very high in this area. As an example, the Daomakan landslide was verified to be triggered by an ancient earthquake. Our results further indicate that the Yaziba Fault has strong activity, and the fault area also has strong seismic activity.

Many paleo earthquakes and several major temblors have been recorded throughout history and many landslides have occurred around the fault, likely caused by seismic ground shaking. All of this information suggests a high level of seismicity in this area. Thus, it is important that we determine if it is possible that a strong earthquake will occur on the Yaziba Fault in the near future. Here, we examine the nearby Longmenshan Fault zone, on which the 2008 *Mw* 7.9 Wenchuan occurred. The near-surface dip angle of the surface rupture produced by this shock was 70°–80°. This is the first event with such a feature that occurred in the interior of the continent in the historical record. Across the world, mostly *M* 8.0 or greater thrust earthquakes occur on large fault zones with slip rates of more than 20 mm/a. The slip rate of the Longmenshan Fault is less than 2 mm/a as evidenced by the geologic and GPS data. Zhang et al. [45] considered that the Yangtze quasi-platform, on which the Sichuan Basin is located, is rigid and is not easily deformed. Thus, it obstructs the horizontal southeastward extension of the Tibetan Plateau. As the boundary between the Tibetan Plateau and the Sichuan Basin, the Longmenshan Fault zone has a high frictional strength and a high angle listric thrust structure. Thus, it is also not easily deformed and is capable of accumulating a large amount of stress. When the accumulated stress exceeds the strength of the fault zone, the fault can rupture suddenly, resulting in large earthquakes such as the 2008 Wenchuan earthquake. The Yingjing-Mabian-Yanjin Fault zone and the Longmenshan Fault zone are both located in the transitional region between the Tibetan Plateau and the Yangtze quasi-platform and have similar thrust nappe structures. The Yaziba Fault in the Yingjing-Mabian-Yanjin Fault zone also has a large dip angle of 70°–80°. Furthermore, the slip rate of the Yingjing-Mabian-Yanjin Fault zone is very low, indicating very weak tectonic deformation [42, 46]. In light of the adjacent Longmenshan Fault zone, the small slip rate of the Yingjing-Mabian-Yanjin Fault zone does not mean that it is stable, but rather that it is likely slowly accumulating elastic strain. Therefore, we conclude that there is a high probability of strong earthquakes occurring in the near future, especially on the Yaziba Fault.

Since the northern end of the Yaziba Fault intersects the Jinsha River, once an earthquake occurs on the fault, many landslides may be induced on both sides of the river. These landslides will slide into the Jinsha River, resulting in secondary disasters such as surges and barrier lakes, which will seriously endanger the people in this region and the safety of the two giant hydropower stations. It should be noted that due to the construction of the Xiangjiaba hydropower station, a new migration village called Qingping County, which contains thousands of migrants, has been settled on the northern end of the Yaziba Fault (Figures 2 and 5(d)). Therefore, the risk assessment of earthquakes and geological hazards in the Qingping County area is necessary. Since the rocks in this region are limestone and basalt, their strength

reduction is lower after they are saturated, so the influence of reservoir impoundment on slope stability is lower than that of an earthquake. Therefore, more attention should be paid to the study of the Yaziba Fault's activity. The results of this study provide useful information for risk assessment and disaster prevention.

6. Conclusions

Through our research, four new findings about the Yaziba Fault and the fault area are put forward. (1) Our field investigations provide new evidence for the northward extension of the Yaziba Fault by 20 km along the Jinsha River in southwestern China. (2) Based on our analysis of new and previously published dates, we conclude that the time interval between earthquakes has shortened from 147,000 to 3,800 years ago. In addition, the historical earthquake records from 1216 to the present indicate a high seismicity around the fault in recent years. (3) Based on remote sensing interpretations, a large number of landslides have been identified in the fault area, with the LND reaching 0.1 km^{-2} and the LAP reaching 0.07, which are higher than those of most mountainous areas. In general, the LND and LAP gradually decrease with the increasing distance from the fault, indirectly reflecting the strong activity of the Yaziba Fault. (4) The limit equilibrium calculation shows that the Daomakan landslide required 0.6 g of horizontal seismic acceleration, which confirms the strong activity of the Yaziba Fault.

Paleo earthquake data are useful for long-term earthquake prediction and the study of fault activity. Based on the results of geologic dating methods and the analysis of ancient landslides associated with seismic ground shaking, it is possible to identify more paleo earthquakes around active faults. These results provide valuable information for the assessment of seismic hazards. This study investigated the area around the Yaziba Fault and identified 19 paleo earthquakes based on 39 geological dating of fault material and nearby landslide artifacts. Considering the fault's scale, the amount of data obtained is still not enough. In the future, we should collect and analyze more data to identify additional paleo earthquakes in this area.

Data Availability

The chronological data and landslides used to support the findings of this study are all included within the article.

Conflicts of Interest

The authors declare that they have no conflicts of interest.

Acknowledgments

This research was supported by the National Key Research and Development Program of China (2018YFC1505004), the National Natural Science Foundation of China (41807267 and 41661144037), and the University Natural Science Research Project of Anhui Province (501100009558). We thank Fuchu Dai of Beijing University of Technology for his field investigation.

References

[1] F. C. Dai, C. Xu, X. Yao, L. Xu, X. B. Tu, and Q. M. Gong, "Spatial distribution of landslides triggered by the 2008 *Ms* 8.0 Wenchuan earthquake, China," *Journal of Asian Earth Sciences*, vol. 40, no. 4, pp. 883–895, 2011.

[2] C. Xu, Y. Tian, B. Zhou, H. Ran, and G. Lyu, "Landslide damage along Araniko highway and Pasang Lhamu highway and regional assessment of landslide hazard related to the Gorkha, Nepal earthquake of 25 April 2015," *Geoenvironmental Disasters*, vol. 4, no. 1, p. 14, 2017.

[3] D. H. Yang, X. X. Yang, and C. Liu, "Global low temperature, earthquake and tsunami (December 26, 2004) in Indonesia," *Progress in Geophysics*, vol. 21, no. 3, pp. 1023–1027, 2006, in Chinese.

[4] D. H. Yang, D. B. Yang, and X. X. Yang, "The influence of tides and earthquakes in global climate changes: Chinese," *Journal of Geophysical Research*, vol. 54, no. 4, pp. 926–934, 2011, in Chinese.

[5] F. C. Dai, C. F. Lee, J. H. Deng, and L. G. Tham, "The 1786 earthquake-triggered landslide dam and subsequent dam-break flood on the Dadu River, southwestern China," *Geomorphology*, vol. 65, no. 3-4, pp. 205–221, 2005.

[6] H. J. Chai, H. C. Liu, and Z. Y. Zhang, "Landslide dams induced by Diexi earthquake in 1933 and its environmental effect," *Journal of Geological Hazards and Environment Preservation*, vol. 6, no. 1, pp. 7–17, 1995, in Chinese.

[7] P. Cui, Y.-Y. Zhu, Y.-S. Han, X.-Q. Chen, and J.-Q. Zhuang, "The 12 May Wenchuan earthquake-induced landslide lakes: distribution and preliminary risk evaluation," *Landslides*, vol. 6, no. 3, pp. 209–223, 2009.

[8] A. C. Graham, K. D. Morell, L. J. Leonard, C. Regalla, and V. Levson, *Field Mapping, LiDAR Analysis and Shallow Geophysical Methods Define the Geometry and Kinematics of the Leech River Fault, an Active Forearc Structure in Northern Cascadia*, American Geophysical Union, Washington, DC, USA, 2016.

[9] A. A. Barka and K. Kadinsky-Cade, "Strike-slip fault geometry in Turkey and its influence on earthquake activity," *Tectonics*, vol. 7, no. 3, pp. 663–684, 1988.

[10] R. Vojtko, F. Marko, F. Preusser, J. Madarás, and M. Kováčová, "Late quaternary fault activity in the Western Carpathians: evidence from the Vikartovce fault (Slovakia)," *Geologica Carpathica*, vol. 62, no. 6, pp. 563–574, 2011.

[11] G. Yielding, J. A. Jackson, G. C. P. King, H. Sinvhal, C. Vita-Finzi, and R. M. Wood, "Relations between surface deformation, fault geometry, seismicity, and rupture characteristics during the El Asnam (Algeria) earthquake of 10 October 1980," *Earth and Planetary Science Letters*, vol. 56, pp. 287–304, 1981.

[12] Q. T. Li, "Present condition and prospects of quantitative assessment on the degree of fault activities: recent developments in world seismology," *Recent Developments in World Seismology*, vol. 5, pp. 1–5, 1994, in Chinese.

[13] S. Topal, "Quantitative analysis of relative tectonic activity in the Acıgöl fault, SW Turkey," *Arabian Journal of Geosciences*, vol. 11, no. 9, p. 198, 2018.

[14] J. Hubbard and J. H. Shaw, "Uplift of the Longmen Shan and Tibetan Plateau and the 2008 Wenchuan ($M = 7.9$) earthquake," *Nature*, vol. 458, no. 7235, pp. 194–197, 2009.

[15] J. Ren, X. Xu, S. Zhang et al., "Surface rupture of the 1933 *M* 7.5 diexi earthquake in eastern tibet: implications for seismogenic tectonics," *Geophysical Journal International*, vol. 212, no. 3, pp. 1627–1644, 2018.

[16] Z. Dai, F. Wang, Q. Cheng et al., "A giant historical landslide on the eastern margin of the Tibetan plateau," *Bulletin of Engineering Geology and the Environment*, vol. 78, no. 3, pp. 2055–2068, 2018.

[17] G. T. Hancox and N. D. Perrin, "Green Lake Landslide and other giant and very large postglacial landslides in Fiordland, New Zealand," *Quaternary Science Reviews*, vol. 28, no. 11-12, pp. 1020–1036, 2009.

[18] N. Wechsler, O. Katz, Y. Dray, I. Gonen, and S. Marco, "Estimating location and size of historical earthquake by combining archaeology and geology in Umm-El-Qanatir, Dead Sea Transform," *Natural Hazards*, vol. 50, no. 1, pp. 27–43, 2009.

[19] J. W. Bell, J. N. Brune, T. Liu, M. Zreda, and J. C. Yount, "Dating precariously balanced rocks in seismically active parts of California and Nevada," *Geology*, vol. 26, no. 6, pp. 495–498, 1998.

[20] R. W. Jibson, "Use of landslides for paleoseismic analysis," *Engineering Geology*, vol. 43, no. 4, pp. 291–323, 1996.

[21] W. Long, J. Chen, P. F. Wang, C. Xu, H. Liu, and J. Z. Sun, "Formation mechanism and back analysis of paleoseismic parameters of Temi large-scale ancient landslide in the upper Jinsha River," *Journal of Seismological Research*, vol. 38, no. 4, pp. 568–575, 2015, in Chinese.

[22] K. Oded and C. Onn, "The geotechnical effects of long human habitation (2000ᶜ years) earthquake induced landslide hazard in the city of Zefat, Northern Israel," *Engineering Geology*, vol. 95, no. 3-4, pp. 57–78, 2007.

[23] T. Fukuchi, "Assessment of fault activity by ESR dating of fault gouge; an example of the 500 m core samples drilled into the Nojima earthquake fault in Japan," *Quaternary Science Reviews*, vol. 20, no. 5–9, pp. 1005–1008, 2001.

[24] S. Ivy-Ochs, S. Martin, P. Campedel et al., "Geomorphology and age of the Marocche di Dro rock avalanches (Trentino, Italy)," *Quaternary Science Reviews*, vol. 169, pp. 188–205, 2017.

[25] Y. Pasqual, J. Peng, and G. Wang, "Characteristics and genetic mechanism of the Cuihua Rock Avalanche triggered by a paleo-earthquake in Northwest China," *Engineering Geology*, vol. 182, pp. 88–96, 2014.

[26] J. Chen, F. Dai, T. Lv, and Z. Cui, "Holocene landslide-dammed lake deposits in the Upper Jinsha River, SE Tibetan Plateau and their ages," *Quaternary International*, vol. 298, pp. 107–113, 2013.

[27] P. Wang, J. Chen, F. Dai et al., "Chronology of relict lake deposits around the Suwalong paleolandslide in the upper Jinsha River, SE Tibetan Plateau: implications to holocene tectonic perturbations," *Geomorphology*, vol. 217, pp. 193–203, 2014.

[28] S. Ivy-Ochs, H.-A. Synal, C. Roth, and M. Schaller, "Initial results from isotope dilution for Cl and ^{36}Cl measurements at the PSI/ETH Zurich AMS facility," *Nuclear Instruments and Methods in Physics Research Section B: Beam Interactions with Materials and Atoms*, vol. 223-224, pp. 623–627, 2004.

[29] S. Ivy-Ochs, A. V. Poschinger, H.-A. Synal, and M. Maisch, "Surface exposure dating of the flims landslide, Graubünden, Switzerland," *Geomorphology*, vol. 103, no. 1, pp. 104–112, 2009.

[30] A. Claude, S. Ivy-Ochs, F. Kober, M. Antognini, B. Salcher, and P. W. Kubik, "The Chironico landslide (Valle Leventina, southern Swiss Alps): age and evolution," *Swiss Journal of Geosciences*, vol. 107, no. 2-3, pp. 273–291, 2014.

[31] China Geological Survey, *Standard for Investigation and Evaluation of Active Faults and Regional Crustal Stability (DD2015-02)*, China Geological Survey, Beijing, China, 2015.

[32] H. D. Lin, *Research Report on Basic Earthquake Intensity of Xiangjiaba Hydropower Station on Jinsha River*, China Earthquake Administration, Beijing, China, 1990.

[33] Z. H. Hou, D. R. Han, F. X. Li, and N. C. Zhong, *Research on Paleo-Earthquake in Late Quaternary along the Northern Part of Qujing-Zhaotong Fault, Yunnan Province*, pp. 3–8, Bulletin of the Institute of Crustal Dynamics, Beijing, China, 1999, in Chinese.

[34] Y. B. Wang, *Comprehensive Study Report on Earthquake of Xiluodu Hydropower Station on Jinsha River*, China Earthquake Administration, Beijing, China, 1990.

[35] Y. Cui, J. Deng, and C. Xu, "Volume estimation and stage division of the Mahu landslide in Sichuan Province, China," *Natural Hazards*, vol. 93, no. 2, pp. 941–955, 2018.

[36] C. Xu, X. Xu, X. Yao, and F. Dai, "Three (nearly) complete inventories of landslides triggered by the may 12, 2008 wenchuan *Mw* 7.9 earthquake of China and their spatial distribution statistical analysis," *Landslides*, vol. 11, no. 3, pp. 441–461, 2014.

[37] C. Xu, X. Xu, and J. B. H. Shyu, "Database and spatial distribution of landslides triggered by the Lushan, China *Mw* 6.6 earthquake of 20 April 2013," *Geomorphology*, vol. 248, pp. 77–92, 2015.

[38] J. Zhuang, J. Peng, C. Xu et al., "Distribution and characteristics of loess landslides triggered by the 1920 Haiyuan Earthquake, Northwest of China," *Geomorphology*, vol. 314, pp. 1–12, 2018.

[39] C. Shi-biao and S.-M. Zhang, *Engineering Geology Manual*, China Building Industry Press, Beijing, China, 4th edition, 2007, in Chinese.

[40] C. S. Liu, "A preliminary study of the Mabian earthquake swarm in Sichuan from 1935 to 1936," *Shanghai Land & Resources*, vol. 2, pp. 58–66, 1986, in Chinese.

[41] G. F. Li and W. Z. Cheng, "Seismic active characteristics from the pre-earthquakes and post-earthquakes occurred in Yibin-Muchuan," *Earthquake Research in Sichuan*, vol. 3, pp. 50–57, 1997, in Chinese.

[42] S. J. Wang and G. Li, "Quantitative assessment and zonation of regional crustal stability in the Jinshajiang River basin," *Journal of Engineering Geology*, vol. 6, no. 4, pp. 289–300, 1998, in Chinese.

[43] X. Ruan, W. Z. Cheng, H. Z. Qiao, Z. W. Zhang, and Y. Fu, "Research of source parameter and stress state of Mabian-Daguan tectonic zone," *Journal of Seismological Research*, vol. 33, no. 4, pp. 294–300, 2010, in Chinese.

[44] W. Z. Cheng, "The reservoir induced earthquake problem in the high intensity area," *Recent Developments in World Seismology*, vol. 4, pp. 10–18, 2013, in Chinese.

[45] P. Z. Zhang, S. B. Zhu, Z. Q. Zhang, and Q. L. Wang, "Seismogenic structure and rupture mechanism of the *Ms* 8.0 Wenchuan earthquake," *Seismology and Geology*, vol. 34, no. 4, pp. 566–575, 2012, in Chinese.

[46] P. Z. Zhang, "The present-day tectonic deformation , strain partitioning and deep dynamic process of the western Sichuan region along eastern margin of Qinghai-Tibet Plateau," *Science in China: Series D*, vol. 38, no. 9, pp. 289–300, 2008, in Chinese.